

## The Instability and Processing Maps of Martensitic Heat Resistant Steels during Hot Deformation

Wenfeng Zhang<sup>a</sup>

School of Mechanical Engineering, Guilin University of Aerospace Technology, Guilin, Guangxi, 541004, China

<sup>a</sup>wfzhang11b@alum.imr.ac.cn

### Abstract

The instability domain appeared around the critical strain for both P92 and NS steels and then phased out after the first stress peak wave. However, unlike the 10Cr steel which exhibited huge instability regions in most part of the contour maps at each strain, 9Cr steel showed great workability during the whole deformation process. Three typical characteristics of microstructure including equiaxed-grain microstructure, stripe microstructure and martensitic-ferritic blend microstructure were found to be associated with the formation of three different processing regions in the contour maps respectively, such as superplastic region, plastic region and failure region.

### Keywords

Hot Deformation, Instability, Processing Maps, Heat Resistant Steels..

### 1. Introduction

The workability consists of two independent parts: state-of-stress (SOS) workability and intrinsic workability [1]. The SOS workability is governed by the geometry of deformation zone and the externally imposed stress state, both of which vary with the different metal deformation processes. The intrinsic workability is decided by the microstructure evolution under certain deformation conditions [2] (different temperature, strain rate, and strain) which is implicitly in the flow stress curves of material. The intrinsic workability is sensitive to the initial microstructure. In recent years, processing maps are regarded as a good method to analyze the workability of metal [3,4].

The martensitic heat resistant steels are assumed to be the most competitive candidates for the USC application at 650 °C thanks to their high heat conductivity, nice thermal fatigue resistance and high stress corrosion resistance [5]. The contour maps of efficiency of power dissipation with instability regions in them at different strains are also drew to avoid the instable deformation which may cause a potential failure in the future use. Finally, the microstructure evolution as a function of  $T$  and  $\dot{\epsilon}$  is illustrated to demonstrate the effect of softening mechanisms on the microstructure development and explain the cause of instable regions.

### 2. Experiment

This study was conducted on four types of martensitic heat resistant steels. The chemical compositions of the experimental steels are listed in Table 1. Bars for the compression test, cut from the slab perpendicular to the forging direction, were machined into samples of 8 mm in diameter and 12 mm in gauge length.

Table 1. Chemical compositions of the experimental steels, wt%

Steel	C	Si	Mn	Cr	Mo	W	V	Nb	B	Co	N
NS	0.021	0.09	1.25	9.37	-	1.42	0.15	0.06	-	-	0.037
P92	0.11	0.37	0.46	8.77	0.42	1.73	0.17	0.057	0.0028	-	0.048
9Cr	0.089	0.31	0.50	8.58	0.40	1.65	0.18	0.060	0.0022	1.64	0.040
10Cr	0.088	0.31	0.50	10.42	0.40	2.55	0.18	0.056	0.0022	2.19	0.058

The rob samples were homogenized in vacuum at 1200 °C for 5 min, and then cooled down to the deformation temperature of 900-1200 °C at a cooling rate of 10 °C/s. After stabilizing holding for 1 min at the deforming temperature, the compression testing samples were deformed to 60% at the strain rate range of 10<sup>-3</sup>-100 s<sup>-1</sup>. The samples were quenched to room temperature as soon as the compressions were finished.

### 3. Results

#### 3.1 Instability and processing maps

The processing map is very effective to describe a deformation behavior in the term of power dissipation ratio  $\eta$ . The parameter  $\eta$  was expressed as following [6] when  $m$  is independent on the strain rate.

$$\eta = \frac{J}{J_{\max}} = \frac{m\sigma\dot{\epsilon} / (m+1)}{\sigma\dot{\epsilon} / 2} = \frac{2m}{m+1} \quad (1)$$

where  $m$  denoted the strain rate sensitivity.  $J$  implied the power dissipated by microstructure changes. As common understanding, the variation  $\eta$  changed with the deformation temperature and strain rate. It is generally expected that the maximum value of  $\eta$  implies the optimum hot working condition for the deformation. However, it is not always pertinent so that high value of  $\eta$  may also result from wedge cracking which is a kind of flow instability. In order to elicit the instability condition during hot deformation, Eq. 2 was proposed by Ziegler [5].

$$\xi(\dot{\epsilon}) = \frac{\partial \ln[m / (m+1)]}{\partial \ln(\dot{\epsilon})} + m > 0 \quad (2)$$

The variation of  $\xi(\dot{\epsilon})$  with temperature and strain rate changing yielded an instability map in which the instability regions were characterized by negative values of  $\xi(\dot{\epsilon})$ . Figure 1 illustrated a three dimensional power dissipating map for the 9Cr steel at the strain of 0.3 along with the dissipation contours and the instability shadow region at the bottom reflection.

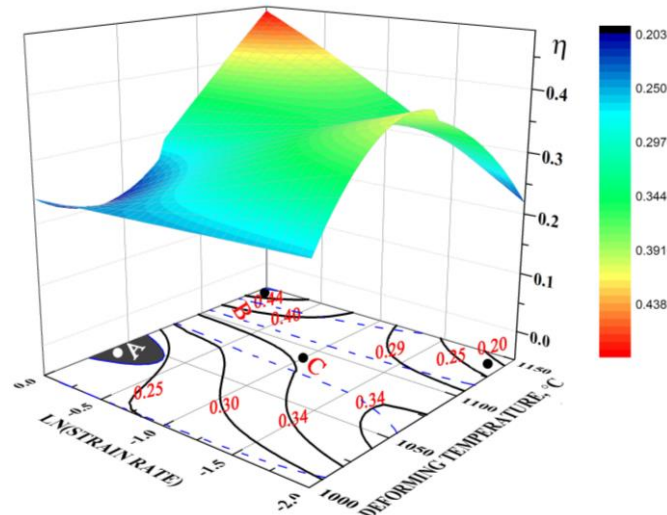


Figure. 1 Three dimensional power dissipating map of 9Cr steel at the strain of 0.3 Conclusion

The instability map of the 9Cr steel had three typical regions marked as A, B and C in Figure 1. The distribution of three typical regions were somehow associated with the efficiency of power dissipation. For instance, region A (the instability domain), where  $\xi(\dot{\epsilon})$  was negative, had a small value of  $\eta$ . The region A was expected to be associated with low workability and was assumed that no noticeable dynamic softening process occurred. However, in this case, the DSIT played a significant role in avoiding the nucleation and propagation of wedge crack at the low  $\eta$  value by degrading the strain accumulation during the deformation. The B domain was related to the superplastic deformation with a high  $\eta$  value. It was believed that both DRX and DSIT occurred. However, there

was no distinct evidence to prove that DRX happened in DSIT ferrite in C region. Instead, the DSIT ferrite in C region displayed stripe shape with wide width along the prior austenite boundaries. The growth of DSIT ferrite caused the main decrease of energy stored during the compression and thus maintains the  $\eta$  value at a relatively high level and consequently better workability in this region than that in the A region.

The efficiency of power dissipation maps along with instability maps of four experimental steels at the strain range of 0.05-0.60 were presented in Figure 2.

It can be seen from Figure 10 that the P92 steel had a good workability after the strain of 0.25 where the flow stress finished its first peak and became stable. None or very small instability region existed before the critical strain for DRX. But it appeared with a certain area at the critical strain and then phased out at the strain of 0.3.

There were very small instability regions in the processing maps for the 9Cr steel because of the augmentation of Co content compared with the commercial P92 steel. With a content of 2 wt% Co, the austenite phase zone was significantly expanded through shrinking the  $\delta$  phase region.

Each map of the 10Cr steel was mainly covered by an instability region due to its high content of alloying elements in austenite during the deformation. The increase of metallic solutes greatly retarded the DRX and made the DRV difficult to happen, by accelerating the stress concentration especially on the triangle boundaries.

The NS steel barely had any instability region above the temperature of 1000 °C and beyond the strain of 0.2. Each of the instability area at different strains was smaller than that of P92 steel owing to the diminishing of C and N content. Both DRX and DRV got prompted due to the reduction of the pinning effect of carbonitrides precipitated during the hot deformation.

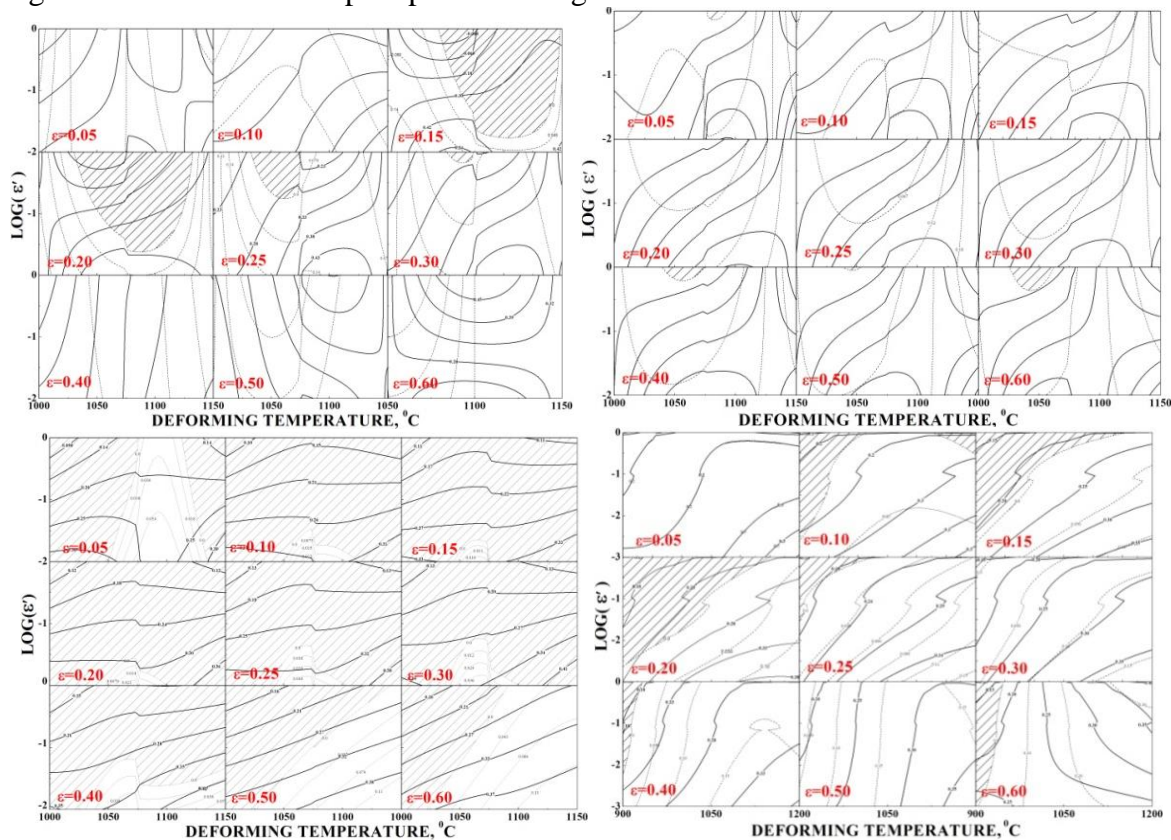


Figure 2. Instability and processing maps at different strain for P92, 9Cr, 10Cr, and NS steels in sequence.

### 3.2 Microstructure evolution

The evolution of microstructure during hot deformation was closely related to DRV, DRX, MDRX and DSIT in the experimental steels. With the change of Z value, the steels exhibited various

microstructure characteristics, as demonstrated in Figure 3. Different softening mechanisms taking in charge under different deformation conditions determined the evolution of microstructure correspondingly.

At high temperature, the DRV got prompted, and the DRX started at a lower strain and proceeded faster, because most of the metallic solutes that usually retard DRV and delay DRX resolved into the matrix [5]. The ferrite grains formed at low temperature and low strain rate (Z value around 40). This was because the nucleation size of the DSIT ferrite was small and the growth of DSIT ferrite was sensitive to both temperature and strain rate. With the strain rate increasing, MDRX governed the subsequent post-dynamic softening gradually.

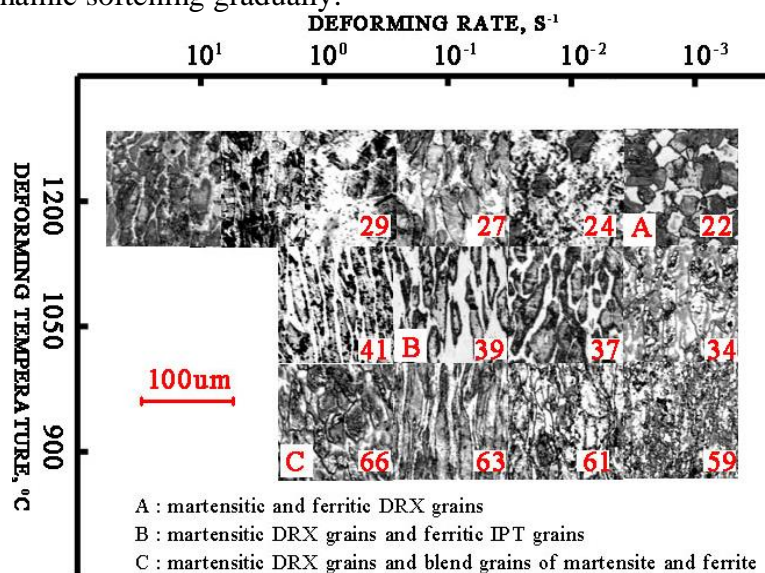


Figure 3. Microstructure evolution and precipitation behavior of NS steel during hot deformation.

#### 4. Conclusion

Beneath the diversity of microstructures and hot deformation processes, it can be concluded that P92 steel manifested good workability after the strain of 0.25. But 9Cr steel had only few instability regions in the processing and instability maps due to the addition of 1.64 wt% Co. Inversely, the addition of Cr and W resulted in large instability domains and poor workability for 10Cr steel. NS steel showed excellent workability owing to the diminution of C and N.

#### Acknowledgements

This work was financially supported by the National Science Foundation for Young Scientists of China (Grant No. 51601044), Guangxi Natural Science Foundation (NO. 2015GXNSFBA139225), Natural Science Foundation of Guilin University Aerospace of Technology (No. YJ1405) and the Dr. Start-up fund for “Study on improving the microstructure stability of the heat resistant steel by modifying the precipitates” from Guilin University Aerospace of Technology.

#### References

- [1] W.F. Zhang, W. Yan, W. Sha, W. Wang, Q.G. Zhou, Y.Y. Shan, K. Yang, Science China Technological Sciences, 55 (2012) 1858-1862.
- [2] W.F. Zhang, P. Hu, W. Yan, W. Sha, W. Wang, Q.G. Zhou, Y.Y. Shan, K. Yang, J Iron Steel Res. Int. supplement 1-1, 18 (2011) 143-147.
- [3] A. I. Fernandez, P. Uranga, B. Lopez, J. Rodriguezibabe., Materials Science and Engineering A, 361 (2003) 367-376.
- [4] A. Marchattiar, A. Sarkar, J.K. Chakravarty, B.P. Kashyap., Journal of Materials Engineering and Performance, (2013).
- [5] P.J. Wray, Metall. Trans. A, 6 (1975) 1197-1199.

- [6] G.R. Stewart, J.J. Jonas, F. Montheillet, ISIJ Int., (2004) 1581–1589.